JOURNAL OF MAGNETIC RESONANCE **124,** 189–199 (1997)
ARTICLE NO. MN961012

Further Developments in MQMAS NMR Spectroscopy for Spin-$\frac{3}{2}$ Nuclei

MELINDA J. DUER* AND CLARE STOURTON

Department of Chemistry, University of Cambridge, Lensfield Road, Cambridge CB2 1EW, Great Britain

Received September 17, 1996

It is shown that multiple-quantum NMR spectroscopy for quadrupolar spins in powder solids gives enhanced resolution over single-quantum spectra for the case of triple-quantum (TQ) NMR for spin-$\frac{3}{2}$. The problem of generating TQ coherence evenly over all molecular orientations is considered and solutions are found. The effects of sample spinning on the excitation of the TQ coherence for spin-$\frac{3}{2}$ is considered in detail. It is shown that selection of a suitable spinning speed is essential if sensible spectra are to be recorded. Finally, it is predicted that the effects of the quadrupole interaction can be removed completely from triple-quantum spectra of spin-$\frac{3}{2}$ by spinning the sample at an angle of 70.1° or 30.6° with respect to the applied field, and experimental results are given. Conclusions derived in this work are applicable to the newly termed *m*ultiple-*q*uantum *m*agic-*a*ngle-*s*pinning experiment.

INTRODUCTION

Some 85% of NMR active nuclei have a spin greater than a half, and therefore possess an electric quadrupole moment. The interaction of such a moment with electric field gradients arising from the surrounding distribution of electrons and nuclei shifts the energy of the nuclear Zeeman spin levels in an NMR experiment, the strength of the interaction depending upon molecular orientation within the applied field (*1*). This results in considerable line broadening in the NMR spectra of these nuclei for solid powder samples, where the quadrupolar interaction is not averaged to its isotropic value by rapid, isotropic molecular motion, as it is in solution samples, for instance. It is probably for this reason that the majority of solid-state NMR is still performed on spin-$\frac{1}{2}$ nuclei, rather than quadrupolar nuclei. However, many chemical problems inevitably involve elements for which there is no convenient spin-$\frac{1}{2}$ isotope, and we must therefore study quadrupolar species. Furthermore, the quadrupolar interaction itself has its uses: it can give information on molecular structure and molecular dynamics in the solid state. Therefore, it would be very convenient to have a technique which allowed quadrupolar-broadened lines from different chemical sites to be resolved, while at the same time retaining information about the quadrupole coupling.

We have recently described (*2*) an experiment which allows the resolution of quadrupolar-broadened lines, while retaining information on the quadrupole interaction, by separating multiple-quantum (MQ) quadrupole powder patterns according to multiple-quantum shifts. Since we first described this technique (*2*), several workers have reexamined the MQ strategy for resolving quadrupolar-broadened lines (*3–6*), which was first explored by Vega and Pines (*7–10*), and later by Wokaun and Ernst (*11*) some 15 years ago. Accordingly, the method has now become known as *m*ultiple-*q*uantum *m*agic-*a*ngle-*s*pinning (MQMAS) NMR. The present paper concentrates on the triple-quantum (TQ) transition of spin-$\frac{3}{2}$, but the principles are equally applicable to the MQ transitions of any spin I. The main aim of this paper is to demonstrate that TQ spectra (and similarly, MQMAS spectra) for spin-$\frac{3}{2}$ systems have significantly improved resolution over single-quantum spectra, while still allowing deduction of the quadrupole parameters. It is for this reason that MQ spectroscopy is expected to find wide applicability in NMR studies of spin-$\frac{3}{2}$ systems and equally in other spin systems. In this work, we also explore the MQMAS technique further than has been done previously and, for instance, consider in detail the effects of sample spinning on the excitation of MQ coherence.

The problem with MQ spectroscopy of quadrupolar nuclei is that the methods of exciting the multiple-quantum coherence used in early work (*7–11*) give amplitudes of coherence which depend upon the strength of the quadrupole interaction. In turn, the strength of the quadrupole interaction de-

* To whom correspondence should be addressed.

1090-7807/97 $25.00

pends upon molecular orientation, and so it has been impossible to generate MQ coherences with even amplitude across all molecular orientations in a powder sample. Furthermore, the unevenness of the MQ generation is very pronounced. Even for an excitation sequence which is optimized for a given quadrupole-coupling constant, some molecular orientations produce no MQ coherence, while others produce an amount which is comparable with the single-quantum coherence produced by a (hard) 90° pulse, for instance. In a sample where there are several different chemical sites, each with a different quadrupole-coupling constant, it is virtually impossible to guarantee that MQ coherences are simultaneously excited for all the sites, let alone to have even generation across the powder patterns for each site. Thus MQ spectra of powder samples obtained by the methods used previously are likely to have ''missing'' signals from some sites, while with other sites, the uneven excitation across molecular orientations makes it impossible to determine the true center of gravity of the powder lineshapes.

In this work therefore, when we investigate methods of generating TQ quadrupolar powder patterns for spin-$\frac{3}{2}$ systems, we keep in mind the need to generate TQ coherence evenly across powder patterns and across sites with different quadrupole-coupling constants. If the TQ coherence is not generated evenly, the resulting MQMAS spectrum will be severely distorted, and quadrupole parameters cannot be obtained from the spectrum. In addition, of course, signal-to-noise will be poor if some molecular orientations do not contribute fully to the spectrum. The investigation here involves both simulations of spectra for different excitation methods (single pulse and 90°—τ—90° sequence) and experimental assessment.

The problem of resolving quadrupolar signals is not new. Two ingenious experiments have been previously devised (*12–17*), which remove the second-order anisotropic quadrupolar broadening from the NMR spectra of central transitions of half-integer spins. The first of these is double rotation (DOR) (*12, 13*). The sample is spun simultaneously about two different axes, one inclined at 54.74° and the other at 70.12° to the applied field. This has the effect of directly averaging the quadrupolar interaction to its isotropic value, providing the rates of spinning about the two axes are large compared to the quadrupolar broadening. The second technique is dynamic-angle spinning (DAS) (*14–17*). This is a two-dimensional experiment where the angle of spinning the sample is stepped between two different values between the t_1 and t_2 periods of the experiment. Both experiments require relatively sophisticated equipment not generally available in an NMR laboratory, and are relatively difficult to implement.

The DOR experiment is designed to eliminate the effects of (anisotropic) quadrupole coupling from the NMR spectrum completely, and, as such, does not retain information that might be useful in studies of the structure and dynamics of a solid. In practice, it is impossible to spin the sample about the two axes sufficiently fast to completely average the quadrupole coupling, and thus spinning sidebands remain, which can reduce the resolution available in the NMR spectrum.

The DAS experiment correlates the isotropic quadrupolar lines with a quadrupole powder pattern, and so information about the quadrupole coupling is retained. For this experiment to give good results, the T_1 spin–lattice relaxation time must be long in order that there be little decay of stored magnetization while the spinning angle is changed. Unfortunately, many quadrupolar nuclei suffer relatively fast spin–lattice relaxation as a result of the large quadrupolar interaction. Furthermore, spin diffusion during the change of spinning angle leads to incomplete refocusing of any dipole–dipole couplings present, and this limits the resolution obtainable from this experiment. Spinning sidebands in the isotropic frequency dimension occur at half the spinning rate, and so even at normal spinning rates, spinning sidebands may appear and may hamper resolution further.

EXPERIMENTAL

Two-dimensional experiments were performed in which TQ coherence evolved in t_1 and was converted to SQ coherence for detection in t_2 by a single pulse, θ_x. Both single-pulse and 90°—τ—90° excitation methods were utilized for exciting TQ coherence. Quadrature detection in t_1 was achieved by performing two experiments, in which the phase of the excitation pulse/pulses was shifted by 30° between the two (*12*). The two resulting datasets are then processed according to the method of Spiess *et al.* (*19*). The TQ spectrum is produced by forming the projection of the two-dimensional dataset on f_1. Alternatively, an MQMAS spectrum could be produced by a shear transformation of the two-dimensional spectrum after Fourier transformation. A three-step phase cycle of the excitation sequence is sufficient to select only ± 3 coherence in t_1. Further phase cycling, as described in Ref. (*4*), for instance, is used to remove T_1 artifacts from f_1. There is no need to phase cycle the last pulse in each sequence, θ_x, which converts the TQ coherence at the end of t_1 into observable SQ coherence in t_2. This final conversion pulse was a pulse of order 2.5 μs, corresponding to $\nu_1\tau_p = 0.25$, in all experiments.

Experiments were performed on ^{23}Na ($I = \frac{3}{2}$) in sodium nitrite and sodium sulfate and a mixture of these two compounds. The ^{23}Na frequency was 105.78 MHz, and all spectra were referenced to solid NaCl at 7.2 ppm, which corresponds to aqueous NaCl at 0 ppm. Samples were spun at the magic

angle at 10 kHz; 256 t_1 slices were collected, with around 100 scans per t_1 slice.

The 90°_x—τ—90°_x sequence was used on the pure $NaNO_2$ and Na_2SO_4 samples. The (nonselective) 90° pulse length was 2.6 μs for $NaNO_2$ and 2.3 μs for Na_2SO_4. Recycle delays were 3 and 10 s, respectively. The τ delay between the two 90° pulses was synchronized with the sample spinning and set equal to one rotor period (100 μs) in length. A second set of experiments was performed on $NaNO_2$ using the 90°—τ—90° sequence described above, but while spinning the sample at 70.12° rather than at the magic angle. These were rotor synchronized in the same way as the previous experiment. The recycle delay was 3 s. Single-pulse excitation was used on an approximately equimolar mixture of $NaNO_2$ and Na_2SO_4. A 5.45 μs pulse, corresponding to $\nu_1\tau_p = 0.5$, was used for the excitation with MAS and the recycle delay was 10 s.

All experiments were performed on a Chemagnetics CMX400 spectrometer, equipped with a double-bearing MAS probehead spinning 4 mm rotors. The spinning speed was controlled, and pulses were synchronized with spinning, using standard Chemagnetics equipment.

THEORY

In exploring different methods of generating TQ coherence for spin-$\frac{3}{2}$, we need to simulate the results expected for different pulse sequences. This section outlines the process of these simulations. It is essential in these simulations to take account of the finite length and amplitude of RF pulses and to take proper account of sample spinning. Previous workers have mainly assumed perfectly hard pulses and/or spinning rates which are large compared with the quadrupole anisotropy. Neither of these situations is achievable in practice in experiments where the quadrupole couplings involved are of the order of megahertz. As is shown later, finite-length pulses and spinning speeds have a tremendous effect on the MQ spectra.

An element ρ_{nm} of the density matrix describing the spin system corresponds to $(n - m)$-quantum coherence. Calculating the time evolution of the density-matrix elements of interest allows us to produce a corresponding FID which is Fourier transformed to give a frequency spectrum for the relevant coherence.

The density matrix $\boldsymbol{\rho}$ is calculated within the Zeeman basis and at any given time t may be calculated from that at time 0 using the solution to the Liouville–von Neumann equation (*20*),

$$\boldsymbol{\rho}(\tau) = \mathbf{U}(\tau)\boldsymbol{\rho}(0)\mathbf{U}^{+}(\tau), \qquad [1]$$

where the propogator matrix $\mathbf{U}(\tau)$ is

$$\mathbf{U}(\tau) = \hat{T}\exp\left[-i\int_0^\tau H(t)dt\right]. \qquad [2]$$

$H(t)$ is the Hamiltonian matrix in the Zeeman basis which describes the spin system at time t. The Hamiltonian matrix does not commute with itself at different times t, so $\mathbf{U}(\tau)$ is calculated recursively using

$$\mathbf{U}(\tau + \delta\tau) = \mathbf{R}^{+}(\tau)\exp[\mathbf{E}(\tau)\delta\tau]\mathbf{R}(\tau)\mathbf{U}(\tau) \qquad \delta\tau \to 0. \qquad [3]$$

$\mathbf{E}(\tau)$ is a diagonal matrix of eigenvalues of $H(\tau)$, and $\mathbf{R}(\tau)$ is the matrix of eigenvectors of $H(\tau)$ (*20, 21*).

Rather than diagonalizing the full Hamiltonian matrix, we form an average Hamiltonian operator to second order over the Larmor period (*20, 24*), of which we consider only the secular terms (*24*). We must consider separately periods of free precession in a pulse sequence and periods where RF pulses are applied, as different effective Hamiltonians operate in these two circumstances. For a period of free precession under sample spinning at an angle θ to the applied field, the effective Hamiltonian operator $H_{fp}(t)$ in the rotating frame (*24, 25*) is

$$\begin{aligned} H_{fp} &= H_Z + H_Q^{(1)} + H_Q^{(2)} \\ &= -\Delta\omega T_{10} + \frac{eQ}{4I(2I-1)h}\sqrt{6}\,V_{20}T_{20} \\ &\quad + \left[\frac{eQ}{4I(2I-1)h}\right]^2 \frac{1}{\omega_L}\left(R_{21}R_{2-1}[T_{21}, T_{2-1}]\right. \\ &\quad \left. + \frac{1}{2}R_{22}R_{2-2}[T_{22}, T_{2-2}]\right). \end{aligned} \qquad [4]$$

The first term describes the effect of the offset $\Delta\omega$ from the Larmor frequency, ω_L. The second term is the first-order quadrupolar term, and the third term is the secular part of the second-order quadrupole term. Expanding the operator commutators and the R products (*25*) in this latter term gives the second-order quadrupolar term in a convenient form,

$$H_Q^{(2)} = -\left[\frac{e^2qQ}{4I(2I-1)}\right]^2 \frac{1}{\omega_L}\frac{2}{5} \times \begin{Bmatrix} (-3\sqrt{10}T_{30} + T_{10}[3 - 4I(I+1)])V_{00} \\ +(-12\sqrt{10}T_{30} - T_{10}[3 - 4I(I+1)])V_{20} \\ +(-34\sqrt{10}T_{30} + 3T_{10}[3 - 4I(I+1)])V_{40} \end{Bmatrix}, \qquad [5]$$

where the T_{k0} operators are irreducible spherical tensor operators,

$$T_{10} = I_z$$
$$T_{20} = \sqrt{\frac{1}{6}}\,[3I_z^2 - I(I+1)]$$
$$T_{30} = \sqrt{\frac{1}{10}}\,[5I_z^2 - 3I(I+1) + 1]I_z \qquad [6]$$

and e^2qQ is the quadrupole-coupling constant, χ, or alternatively (*25*),

$$H_Q^{(2)} = -\frac{2}{\omega_L}\left[\frac{e^2qQ}{4I(2I-1)}\right]^2\{(-3T'_{30} + T'_{10})V_{00} + (-12T'_{30} - T'_{10})V_{20} + (-34T'_{30} + 3T'_{10})V_{40}\}, \qquad [7]$$

where the operators T'_{10} and T'_{30} are defined as

$$T'_{10} = T_{10}\tfrac{4}{5}[\tfrac{3}{4} - I(I+1)]$$
$$T'_{30} = T_{30}\sqrt{\tfrac{2}{5}}. \qquad [8]$$

The V_{k0} terms arise from the quadrupole-coupling tensor. They can be expressed in terms of Wigner rotation matrices which relate the principal-axis frame (PAF) of the quadrupole tensor to a frame attached to the sample rotor and those which relate the rotor frame to the laboratory frame (*22*, *24*),

$$V_{k0} = \sum_m D^{(k)}_{m0}(\omega_R t,\, \theta_R,\, 0) \sum_n D^{(k)}_{nm}(\alpha,\, \beta,\, \gamma)A_{kn}, \qquad [9]$$

where (α, β, γ) are the Euler angles relating the PAF to the rotor frame and $(\omega_R t, \theta_R, 0)$ are those relating the rotor frame to the laboratory frame, ω_R being the sample spinning speed and θ_R the angle that the spinning axis is inclined with respect to the applied field. The A coefficients are given by (*26*)

$$A_{00} = -\frac{1}{5}(3 + \eta^2)$$
$$A_{20} = \frac{1}{14}(\eta^2 - 3),\; A_{2\pm2} = \frac{1}{7}\sqrt{\frac{3}{2}}\,\eta$$
$$A_{40} = \frac{1}{140}(18 + \eta^2),\; A_{4\pm2} = \frac{3}{70}\sqrt{\frac{5}{2}}\,\eta,\; A_{4\pm4} = \frac{1}{4\sqrt{70}}\,\eta^2, \qquad [10]$$

where η is the asymmetry parameter associated with the quadrupole tensor. It has been shown before that in general, nonsecular terms in a spin Hamiltonian have only a very small effect on lineshapes (*21*).

During a pulse, we must consider contributions from Zeeman, quadrupole, and radiofrequency interactions with the spin. The second-order average Hamiltonian during a pulse, H_p, is thus given by the Hamiltonian in Eqs. [4]–[8] plus a term which accounts for the effects of the RF pulse, H_{RF}:

$$H_p = H_{fp} + H_{RF} = H_{fp} + \frac{\omega_1}{\sqrt{2}}\,[T_{1-1}\exp(+i\phi) - T_{11}\exp(-i\phi)]. \qquad [11]$$

ω_1 is the amplitude of the RF pulse and ϕ its phase. The tensor operators are defined as

$$T_{1\pm1} = \mp\sqrt{\tfrac{1}{2}}I_\pm. \qquad [12]$$

For each pulse and free precession period in the pulse sequence, the period is split into N sequential time points, and the appropriate Hamiltonian matrix is constructed for each time point, using Eq. [4] or [11]. The so-constructed series of Hamiltonian matrices is then used recursively in Eq. [3] to calculate the propogator $\mathbf{U}$. In practice, the number N of time points in each period must be increased until further increase in N gives insignificant change to the final calculated density matrix.

THE APPEARANCE OF TQ SPECTRA FOR SPIN-$\frac{3}{2}$

We wish to show how the MQ powder spectra of quadrupolar nuclei can be used to resolve signals which overlap in the single-quantum (SQ) spectrum and furthermore how they can be used to determine the quadrupole parameters associated with those signals. In this section, we assess the orientation dependence of the TQ transition frequency for spin-$\frac{3}{2}$ and hence predict the appearance of TQ NMR spectra for powder samples. We also determine the second-order quadrupolar isotropic shift for the TQ transition and compare it with that for the SQ transition. Simple application of the expressions for the first- and second-order energy corrections arising from perturbation theory for the Zeeman spin states perturbed by quadrupole coupling (*1*, *2*) shows that, to first order, the TQ transition for a spin-$\frac{3}{2}$ is not affected by the quadrupole interaction. Indeed, this is generally the case for all $+m \rightarrow -m$ transitions for any half-integer spin. However, those same expressions show that the TQ transition is affected by the quadrupole coupling to second order, and therefore, that the TQ transition frequency depends upon molecular orientation at this level of approximation.

The perturbation-theory expressions for energy corrections to the Zeeman levels (*1*) for a spin at a site of axial symmetry in a nonspinning sample can be used to show that the orientation dependence of the TQ transition frequency for a spin-$\frac{3}{2}$ can be expressed by fourth-rank spherical harmonics only. This is in contrast to the general situation for quadrupolar transition frequencies, where the orientation dependence must be described by a linear combination of both second- and fourth-rank spherical harmonics, if the second-order effects of quadrupole coupling are significant (*13, 17, 24*). This result for the TQ transition of spin-$\frac{3}{2}$ can be extended to the more general case of a spin at a site of nonaxial symmetry in a spinning sample, by application of Eq. [4] above. We use the secular, second-order effective Hamiltonian of Eq. [4] describing the Zeeman and quadrupole interactions to derive an expression for the frequency of the TQ transition for a spin-$\frac{3}{2}$, ν_{TQ},

$$\nu_{TQ} = 3\Delta\nu - \left[\frac{e^2qQ}{4I(2I-1)}\right]^2 \frac{1}{\nu_L}\{18V_{00} + 84V_{40}\} \quad [13]$$

which may be rewritten as

$$\nu_{TQ} = 3\Delta\nu + \frac{\chi^2}{40\nu_L}(3+\eta^2) - \frac{7}{12}\sum_m D^{(4)}_{m0}(\omega_R t, \theta_R, 0)\sum_n D^{(4)}_{nm}(\alpha, \beta, \gamma)A_{4n}, \quad [14]$$

where the A coefficients and χ (the quadrupole-coupling constant) were defined previously. The first term in Eq. [13] is the Zeeman offset, and the second is from the second-order quadrupole coupling showing, as expected, the dependence on fourth-rank Wigner rotation matrices only. Equation [14] expresses the isotropic part of the TQ frequency explicitly, with the second term being the second-order isotropic quadrupolar shift for the TQ transition.

It is then interesting to compare the isotropic shift in the TQ spectrum with that expected for the single-quantum $+1/2 \rightarrow -1/2$ spectrum for spin-$\frac{3}{2}$. The total isotropic shift for the SQ transition is (*13, 17*)

$$\nu^i_{SQ} = \Delta\nu - \frac{\chi^2}{120\nu_L}(3+\eta^2) = \Delta\nu - \Delta\nu^i_Q, \quad [15]$$

where

$$\nu^i_Q = \frac{\chi^2}{120\nu_0}(3+\eta^2), \quad [16]$$

while that for the TQ transition is

$$\Delta\nu^i_{TQ} = 3\Delta\nu + 3\Delta\nu^i_Q. \quad [17]$$

The quadrupolar contribution to the isotropic shift in the TQ transition is three times that of the SQ transition and in the opposite sense. The combination of the increased isotropic chemical and second-order quadrupolar shifts in the TQ spectrum should give significantly enhanced resolution in the TQ spectrum over that in the SQ spectrum for spin-$\frac{3}{2}$.

There is the possibility of even greater resolution in the TQ spectrum of a spin-$\frac{3}{2}$ nucleus. Equation [14] shows that the TQ transition frequency depends only upon fourth-rank Wigner rotation matrices. Such a dependence may be averaged out by spinning the sample about an axis inclined at 30.6° or 70.1° to the applied field (*17, 24*). This simple technique should result in a TQ spectrum in which all the anisotropic effects of quadrupole coupling are removed. Of course, spinning at either of these angles does not completely remove the effects of any chemical-shift anisotropy or dipole–dipole coupling. However, the latter may be removed by a variety of multiple-pulse sequences (*20*).

GENERATION OF MULTIPLE-QUANTUM COHERENCES

The study of quadrupolar nuclei in solids has always been plagued by the problem of generating a given coherence equally for all values of quadrupole coupling (*7–11, 28–34*). This is equally problematic if we wish to record MQ powder patterns (in the f_1 domain of a two-dimensional experiment, for instance) or produce an MQMAS spectrum (*3, 4*). For the latter, a useful SQ powder pattern, from which quadrupole parameters can be determined, cannot be obtained from the experiment without even generation of the corresponding MQ coherence over all molecular orientations. Furthermore, signal intensity will be lacking if some molecular orientations contribute only weakly to the spectrum.

For a static sample, the first-order quadrupole frequency, ω_Q, is

$$\omega_Q = \frac{e^2qQ}{4I(2I-1)}[(3\cos^2\theta - 1) + \eta\sin^2\theta\cos 2\phi], \quad [18]$$

where the angles θ and ϕ describe the orientation of the quadrupole PAF with respect to the applied field. In general, if the amplitude of the irradiating RF pulse, ω_1, is less than or of order of ω_Q, then the amplitude of any coherence generated depends upon ω_Q (*7–11, 28–34*). Only if short, hard pulses are used (*32, 34*) can this dependence be avoided. The quadrupole frequency ω_Q depends on molecular orienta-

tion, and so if the amplitude of a coherence generated by a pulse depends upon ω_Q, the result is that the coherence cannot be generated with equal amplitude for all the orientations in a powder sample, for instance, let alone be generated equally for sites with different quadrupole-coupling constants to start with.

Vega and Naor (*10*) have shown rigorously that in the case of a weak pulse ($\omega_1 \ll \omega_Q$), the effective RF irradiation intensity for an *n*-quantum transition is proportional to $\omega_1^n/\omega_Q^{n-1}$. It is clear that such a dependence gives rise to gross distortions of the expected quadrupolar powder lineshapes for powder samples, since ω_Q is zero, for instance, for some molecular orientations. Clearly, the problem of even irradiation of a given *n*-quantum transition is something which must be addressed if we are to perform any form of spectroscopy on quadrupolar nuclei, but particularly, MQ spectroscopy.

Since the problem is essentially that we wish to remove the molecular orientation dependence from the MQ excitation profile, one solution is to arrange for the molecular orientation to be averaged during the excitation. This can of course be arranged in part by simply spinning the sample. We have therefore investigated various methods of exciting MQ coherences which include sample spinning to ''smooth'' the excitation profile. We concentrate here on the generation of TQ coherence for spin-$\frac{3}{2}$, although it is to be emphasized that the results presented have general applicability for the generation of any coherence for any quadrupolar spin.

MQ coherences are generated in coupled spin systems in solution by a 90°_ϕ—τ—$90^\circ_{\phi+\phi'}$ sequence, often with a 180° pulse at the center of the τ period to refocus any chemical-shift offsets. The τ delay is generally set to be the inverse of the coupling strength in hertz for optimal MQ excitation. We therefore investigate this pulse sequence with sample spinning as a general method for exciting TQ coherence for spin-$\frac{3}{2}$.

Vega and Naor (*10*) have shown that a single weak pulse may be used generate TQ coherence in the case where $\omega_1 \ll \omega_Q$, although they point out the large orientation dependence of this method. Thus, we investigate this method, again focusing on the effects of sample spinning.

90°—τ—90° Sequence

In order to best understand the origins of the results in this section, it is useful to first recap how the 90°—τ—90° pulse sequence generates multiple-quantum coherence. At equilibrium, the density operator for a spin I may be described in terms of the irreducible tensor operator T_{10}. Without loss of generality, we assume that the first (hard) pulse is along *x* in the rotating frame. This creates transverse magnetization and a density operator ρ which in terms of irreducible tensor operators is

$$\rho = -\frac{1}{\sqrt{2}}(T_{11} + T_{1-1}). \qquad [19]$$

During the delay τ, the spin system evolves under the offset and the quadrupole coupling described by the Hamiltonian in Eqs. [4]–[8]. We can use the well-known expansion

$$e^{-\mathbf{A}}\mathbf{B}e^{+\mathbf{A}} = \mathbf{B} - [\mathbf{A}, \mathbf{B}] + \frac{1}{2!}[\mathbf{A}, [\mathbf{A}, \mathbf{B}]] - \frac{1}{3!}[\mathbf{A}, [\mathbf{A}, [\mathbf{A}, \mathbf{B}]]] + \cdots \qquad [20]$$

along with Eqs. [1] and [2] to determine what terms arise in the density operator as a result of this evolution under the quadrupole coupling. The necessary commutation relations between the various T_{kq} tensor operators in ρ and $\mathcal{H}_{fp}$ are conveniently listed in Refs. (*36, 37*). In this manner, it can be shown that the $T_{1\pm1}$ terms of the initial density operator evolve under both the T_{20} and the various T_{30} terms of $\mathcal{H}_Q^{(1)} + \mathcal{H}_Q^{(2)}$ to give $T_{3\pm1}$ terms (among others) in the density operator at a general time *t*. It is these $T_{3\pm1}$ terms which the final 90° pulse of the 90°—τ—90° sequence then converts into the triple-quantum $T_{3\pm3}$ terms (*36, 37*) which evolve during the t_1 period of the experiment.

Further insight into the operation of the 90°—τ—90° sequence is gained if we focus more closely on the formation of these $T_{3\pm1}$ terms in the density operator during the τ delay. The $T_{3\pm1}$ terms which arise from evolution under the T_{30} terms associated with different V_{k0}, $k = 0, 2, 4$, contributions clearly have different orientation dependencies, and likewise, the $T_{3\pm1}$ terms arising from evolution under the T_{20} term of the first-order quadrupole Hamiltonian, $\mathcal{H}_Q^{(1)}$. Thus, the size of the $T_{3\pm1}$ terms which arise in the density operator for a given molecular orientation is determined by contributions from V_{00}, V_{20}, and V_{40}. These various contributions interfere with each other for each molecular orientation, resulting in a very complex overall lineshape for the complete powder sample.

We have simulated the TQ lineshapes using the method outlined in a previous section for spinning at the magic angle and different τ delays. A selection of these are shown in Fig. 1, along with the ideal TQ lineshape assuming equal excitation for all molecular orientations. As expected, the lineshapes are complicated in general, showing phase and amplitude distortions from the ideal lineshape. The exception is when the τ delay is set equal to exactly one rotor period of the sample spinning, τ_R. Here the lineshape shows no phase distortion and only minimal amplitude distortion. It is also significantly more intense than that for other values of τ. The reason for this is that by setting $\tau = \tau_R$ while spinning at the magic angle, only the terms associated with

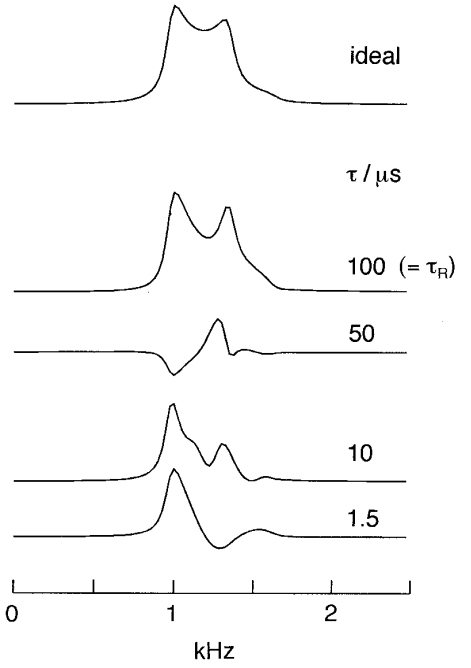

FIG. 1. Illustration of how the TQ lineshape varies with τ when a 90°_x—τ—90°_x excitation sequence is used. Top: Simulation of an ideal TQ powder lineshape for a sample under MAS. The quadrupole-coupling constant is 1.3 MHz; asymmetry, 0; chemical-shift offset, 0 Hz; spectral frequency, 105.7 MHz; sample spinning rate, 10 kHz at the magic angle. Below: Simulations of the TQ lineshape produced by the 90°_x—τ—90°_x pulse sequence for different values of τ for the same quadrupole parameters as above. The 90° pulse length used in the simulations was 2.5 μs (corresponding to $\nu_1\tau_p = 0.25$). The values of τ used are given alongside each simulation.

V_{00} and V_{40} contribute to the $T_{3\pm1}$ terms formed in the density operator. The effects of operators in the effective Hamiltonian with factors of V_{20} are averaged to zero. The result is that there is no interference of $T_{3\pm1}$ terms with different orientation dependencies, i.e., those formed from V_{20} and V_{40} terms (V_{00} is a constant). The same will of course be true if the rate of sample spinning is much larger than the quadrupolar anisotropy, but this is unlikely to be achievable for many systems in practice, with quadrupole-coupling constants of the order of megahertz.

It is worth noting that for $\tau = [3\chi/2I(2I-1)]^{-1}$ (Fig. 1, $\tau = 1.5$ μs), the TQ lineshape is very distorted. This delay, the inverse of the quadrupole-coupling splitting, might be expected to give the maximum amplitude of TQ coherence from experience with solution NMR. However, this work shows that this is not the case. These results show that the 90°—τ—90° sequence is only useful for generating MQ coherence in an MQMAS experiment or other MQ experiments if the delay τ is set equal to an integral number of rotor periods.

Figure 2 shows experimental confirmation of this finding with TQ spectra for ^{23}Na in Na_2SO_4 recorded with (a) $\tau = \tau_R$ (100 μs, 100 kHz sample spinning) and (b) $\tau = \tau_R/2$ (50 μs). The finding was further investigated in another set of experiments. A series of one-dimensional spectra were recorded using the 90°_x—τ—90°_x—t_1—90°_x—t_2 sequence for different τ delays and $t_1 = 0$. In an ideal situation, these spectra would have the central $+1/2 \rightarrow -1/2$ transition lineshape which would be produced with a perfectly hard RF pulse. Distortions from this lineshape are due to (i) imperfect excitation over different molecular orientations of the TQ coherence from which the observed SQ coherence is produced and (ii) imperfect transfer of TQ to SQ coherence. Clearly, in the series of experiments here where τ is the only variable, changes in the lineshape between experiments with different τ are due only to (i). The

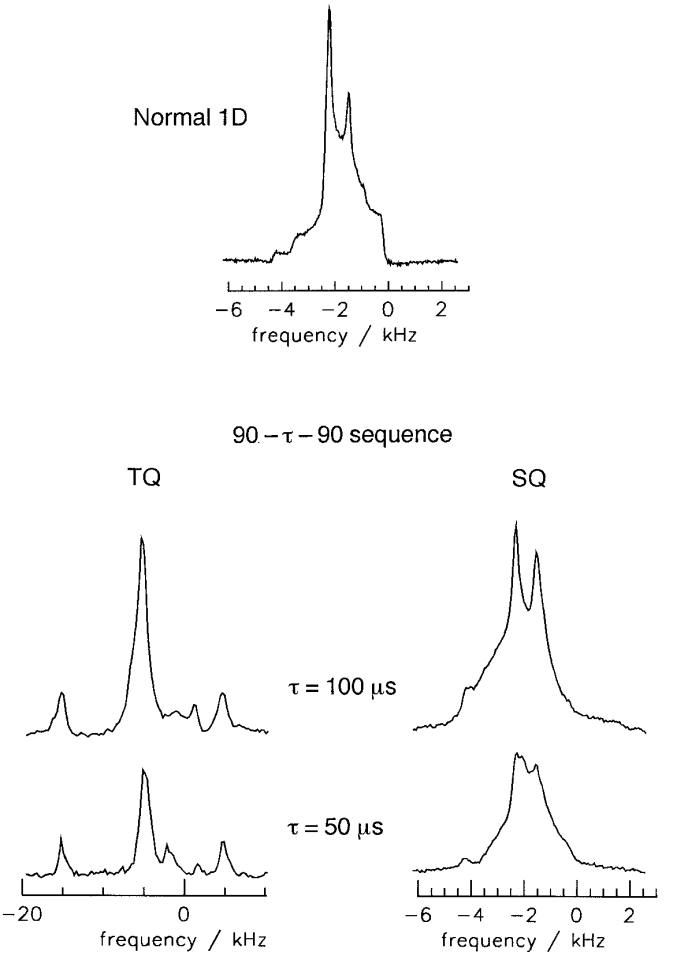

FIG. 2. Top: Central ^{23}Na SQ transition experimental lineshape for Na_2SO_4 recorded in a normal one-dimensional experiment with a $\pi/10$ pulse and 10 kHz sample spinning. Below: Experimental magnitude spectra from two-dimensional TQ experiments for ^{23}Na in Na_2SO_4 recorded with 90°_x—τ—90°_x excitation of TQ coherence for $\tau = 100$ μs ($=\tau_R$) and $\tau = 50$ μs with sample spinning of 10 kHz. Left: Projections of the TQ lineshape on f_1. Right: Projections of the central SQ transition on f_2.

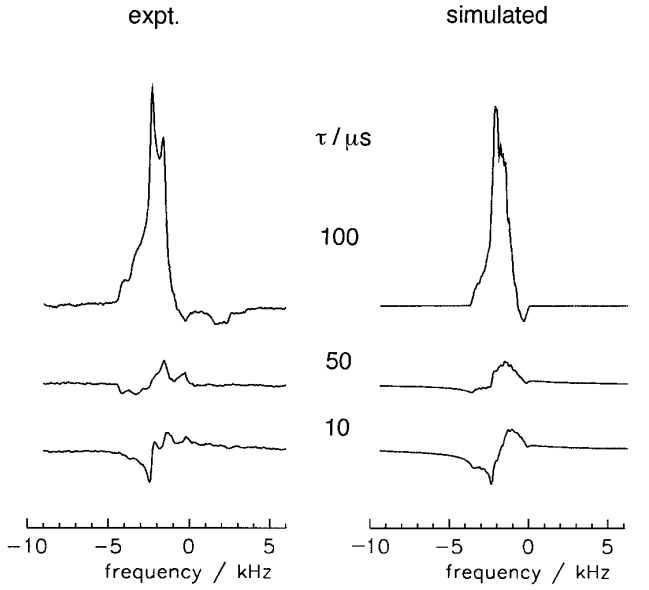

FIG. 3. Left: Experimental f_2 spectra recorded with the 90°_x—τ—90°_x—t_1—90°_x—t_2 pulse sequence for $t_1 = 0$ and different τ delays for ^{23}Na in Na_2SO_4. The optimum value for τ should give a lineshape which closely approximates the central transition lineshape from the single-pulse experiment at the top of Fig. 2. The sample spinning speed was 10 kHz for all spectra. Right: Simulated spectra assuming the above pulse sequence and experimental parameters and literature values for the quadrupole parameters ($\chi = 2.6$ MHz; $\eta = 0.6$) (*17*).

results of some of these experiments are shown in Fig. 3 for Na_2SO_4 along with the ideal central-transition lineshape. All these SQ lineshapes clearly show gross distortions with the exception of that recorded with $\tau = \tau_R$. Furthermore, the intensities of all the spectra with $\tau \neq \tau_R$ are very low in comparison to that for $\tau = \tau_R$ due to cancellations between components of TQ coherence arising from different molecular orientations.

Single-Pulse Excitation

Vega and Naor (*10*) have shown how TQ coherence may be excited for spin-$\frac{3}{2}$ for a single weak ($\omega_1 \ll \omega_Q$) pulse. The amplitude of TQ coherence produced by this method for a static sample is proportional to

$$\sin\left(-\frac{3\omega_1^3}{2\omega_Q^2}\tau_p\right), \qquad [21]$$

where τ_p is the pulse length, and ω_Q has been defined in Eq. [18]. Thus the effective nutation rate of the TQ coherence under the RF pulse is $-3\omega_1^3/2\omega_Q^2$.

Clearly, the ω_Q dependence of the TQ amplitude produced by this method makes it less than ideal for exciting TQ coherence in static powder samples, or in samples where the quadrupole-coupling constant χ differs between chemical sites, as pointed out in the original work (*10*). Frydman *et al.* (*3, 4*) have examined the optimal conditions for a single excitation pulse in the regime of very rapid magic-angle spinning (MAS), i.e., $\nu_R \gg \nu_1$, $|H_Q^{(2)}|$, and we would refer the reader to these excellent papers for further details on the pulse power and angle required for optimal TQ excitation in spin-$\frac{3}{2}$. However, in the majority of cases, the speed of sample spinning is unlikely to be rapid with respect to pulse amplitude ν_1 or even the TQ quadrupolar linewidth. It is therefore important to consider the effects of sample spinning at finite spinning speeds.

We have used the optimal pulse condition proposed by Frydman *et al.* (*4*) of $\omega_1\tau_p/2\pi = 0.8$, where τ_p is the pulse length, and calculated the TQ lineshape produced by such a pulse under MAS of different speeds and for two different pulse amplitudes, $\omega_1/2\pi$. The results are shown in Fig. 4, and are to be compared with the ideal TQ lineshape in Fig. 1. We include in Fig. 4 simulations of the lineshape for the limit where $\nu_R \gg \nu_1$. Clearly, in this limit, recognizable TQ lineshapes are produced. The same occurs when $\nu_R \ll \nu_1$. However, in the regime $\nu_R \sim \nu_1$, very distorted lineshapes are predicted, presumably as a result of the interfering influences of the sample spinning and the RF pulses. Thus if these MAS conditions were to be used in an MQMAS experiment, for instance (*3, 4*), the SQ lineshapes resulting in f_2 would be correspondingly distorted.

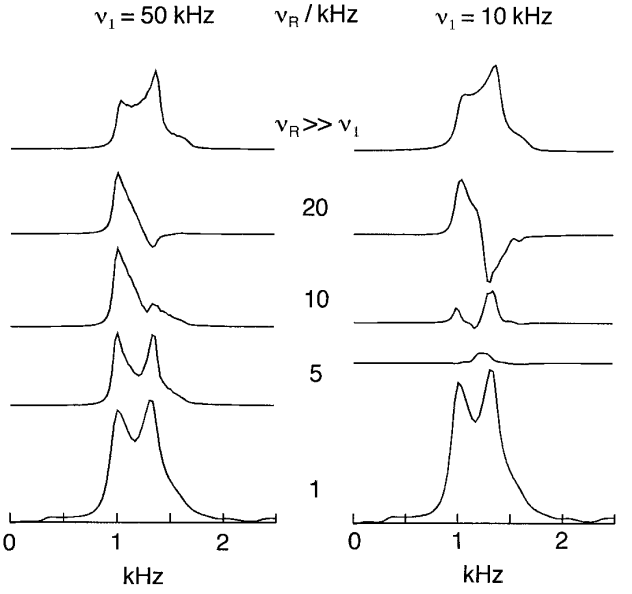

FIG. 4. Simulations of the TQ lineshape arising from a single excitation pulse for two different pulse amplitudes, $\nu_1 = 50$ kHz and $\nu_1 = 10$ kHz, as a function of sample spinning speed. The spectra for $\nu_1 = 10$ kHz have been scaled up by a factor of 5.0 compared with those for $\nu_1 = 50$ kHz. The length of the pulse, τ_p, in each case is determined by $\nu_1\tau_p = 0.8$ cycle. The sample spinning speed is given with each spectrum. The quadrupole parameters are as for Fig. 1. The apparent baseline distortions for the 1 kHz spinning spectra are due to spinning sidebands.

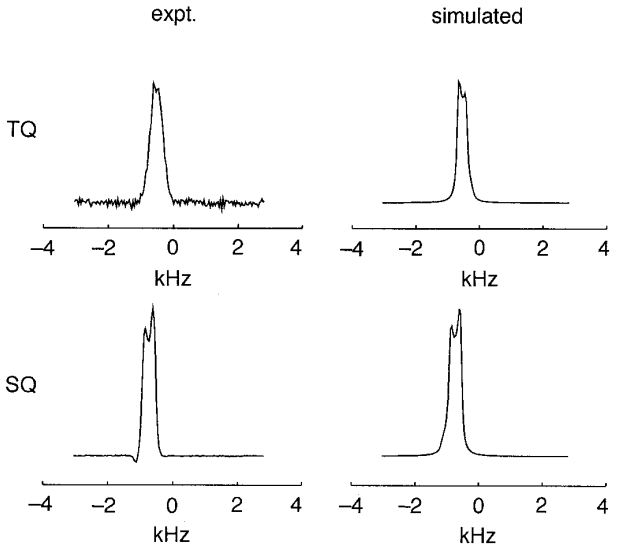

FIG. 5. Results of the two-dimensional TQ ^{23}Na experiment with sample spinning at the magic angle for sodium nitrite. The figure shows both the triple-quantum (TQ) and the single-quantum (SQ), central-transition projections. The 90°_x—τ—90°_x sequence was used to generate the TQ coherence in the experiment. The (nonselective) 90° pulse length was 2.6 μs; the τ delay was 100 μs, which corresponds to one rotor period, i.e., sample spinning at 10 kHz. Alongside the experimental spectra are simulated spectra. These are the ideal TQ and SQ lineshapes, respectively, predicted for a quadrupole-coupling constant of 1.1 MHz; asymmetry, 0.11 [literature data (*37*)]; isotropic chemical shift, −469 Hz; spectral frequency, 105.78 MHz; spinning at 10 kHz at the magic angle.

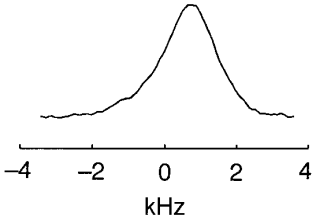

FIG. 6. Results of the two-dimensional TQ ^{23}Na experiment spinning at 70.12° to the applied field for sodium nitrite. The 90°_x—τ—90°_x sequence was again used to generate the TQ coherence. Experimental conditions were the same as those used in Fig. 5 except for the spinning angle and the isotropic chemical-shift offset was arranged to be −109 Hz in the single-quantum spectrum. Using Eq. [17] and the quadrupole parameters used in the simulations of Fig. 5, these conditions would be expected to give rise to an isotropic signal with a shift of +535 Hz. See text for details.

RESULTS AND DISCUSSION

Figure 5 shows the TQ spectrum for $NaNO_2$ produced using the 90°—τ—90° pulse sequence under the magic angle (54.75°), with τ synchronized to the rotor period, and compares it with the SQ spectrum. The quadrupole-coupling constant and asymmetry for ^{23}Na in sodium nitrite have previously been determined (*31*) to be 1.1 MHz and 0.1, respectively. Simulation gives the isotropic chemical-shift offset of the SQ resonance as −469 Hz and that of the TQ resonance as −1407 Hz, which is indeed three times that of the SQ resonance. Furthermore, the TQ lineshape accords well with that expected from theory (Fig. 5, top right).

Figure 6 shows a spectrum equivalent to that described above but for a spinning angle close to 70.1°. This spinning angle should remove all effects of quadrupolar broadening from the TQ spectrum. As can be seen from Fig. 6, however, the TQ line shows considerable line broadening. The effects of dipolar broadening and chemical-shift anisotropy are not averaged to zero by spinning at this angle. Indeed, the line broadening from each of these effects is magnified by a factor of three in the TQ spectrum as compared with the SQ spectrum, and it is presumably these effects which cause the broad line observed experimentally. It may be that a compromise angle between 54.74° and 70.12° would give more useful results. In general, the optimal spinning angle will be determined by the nature of the sample, but spinning at 70.12° is only likely to be useful for samples where homonuclear dipolar coupling is small or if multiple-pulse sequences for the removal of homonuclear dipolar coupling are included in the experiment.

Figures 7 and 8 demonstrate the real utility of the TQ or MQMAS experiment: the greater resolution in the TQ spectrum (and correspondingly in the MQMAS spectrum) over any SQ spectrum. Figure 7 shows the SQ spectrum of central transitions for a mixture of $NaNO_2$ and Na_2SO_4. As Fig. 7 shows, the two ^{23}Na signals expected are not resolved in the SQ spectrum due to the second-order quadrupolar broadening in both compounds.

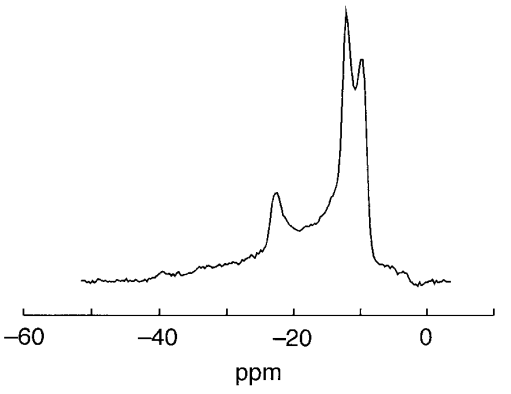

FIG. 7. The SQ ^{23}Na spectrum (central transitions only) from the two-dimensional experiment described in the text for an approximately equimolar mixture of $NaNO_2$ and Na_2SO_4. The frequency scale is relative to solid NaCl at 7.2 ppm (and thus aqueous NaCl at 0 ppm). The ^{23}Na signals from $NaNO_2$ and Na_2SO_4 are not resolved in this spectrum. Simulation using literature values for the quadrupole parameters (*17, 37*) gives the isotropic chemical shifts as −15.8 and −8.6 ppm for $NaNO_2$ and Na_2SO_4, respectively.

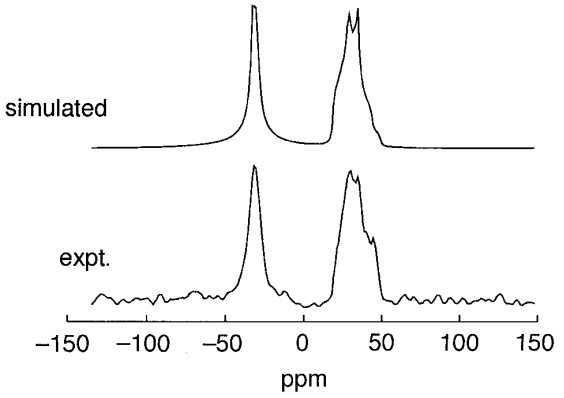

FIG. 8. The TQ ^{23}Na spectrum for the same sample used for Fig. 7. The frequency scale is relative to solid NaCl at 7.2 ppm (and thus aqueous NaCl at 0 ppm). In the experiment, a single pulse (5.9 μs corresponding to $\nu_1\tau_p = 0.5$ cycle) was used to excite the TQ coherence. The simulation of the ideal TQ spectrum for the mixture used literature values for the quadrupole parameters [$NaNO_2$ (*37*), $\chi = 1.1$ MHz; $\eta = 0.11$; and Na_2SO_4 (*17*), $\chi = 2.6$ MHz; $\eta = 0.6$]. The isotropic chemical shifts used were -15.4 and -8.8 ppm for $NaNO_2$ and Na_2SO_4, respectively, which agree well with the values deduced from the SQ spectrum. The intensities of the $NaNO_2$ and Na_2SO_4 simulations were scaled separately to give the best fit to the experimental spectrum.

Figure 8 shows the TQ spectrum recorded for the mixture with magic-angle spinning and single-pulse TQ excitation. The spectrum does indeed show two distinct signals, centered at approximately -30 and $+34$ ppm. Simulations of the TQ lineshapes for $NaNO_2$ and Na_2SO_4 using literature values for the quadrupole-coupling parameters (Fig. 8) accord well with the experimental data. The increased resolution seen in the TQ spectrum is retained if a skew projection of the two-dimensional dataset is taken so as to form an isotropic spectrum in f_1 rather than the TQ spectrum. This feature makes MQ techniques superior to any other techniques producing an isotropic spectrum for quadrupolar nuclei.

CONCLUSIONS

In conclusion, multiple-quantum spectroscopy, including MQMAS, of quadrupolar nuclei offers significant improvements in resolution over conventional single-quantum experiments and still allows the determination of quadrupole parameters. The increased resolution is vital in chemical systems with similar nuclear sites, or where the chemical-shift range of the observed nucleus is small, i.e., ^{7}Li, $I = \frac{3}{2}$.

If sensible and interpretable spectra are to be obtained, it is essential that MQ coherence be generated equally (or nearly so) for all molecular orientations. We have shown that both 90°—τ—90° and single-pulse excitation methods, both with sample spinning, can be used to excite MQ coherences in powder samples. However, the experimenter must exercise care in the selection of spinning speed with both methods. In particular, the 90°—τ—90° method is only useful with τ set equal to τ_R.

REFERENCES

1. A. Abragam, ''Principles of Nuclear Magnetism,'' Clarendon Press, Oxford, 1961.
2. M. J. Duer and E. C. Stourton, 35th Experimental NMR Conference, Pacific Grove, California, Poster WP222, 1994.
3. L. Frydman and J. S. Harwood, *J. Am. Chem. Soc.* **117,** 5367 (1995).
4. A. Medek, J. S. Harwood, and L. Frydman, *J. Am. Chem. Soc.* **117,** 12779 (1995).
5. D. Massiot, B. Touzo, D. Trumeau, J. P. Coutures, J. Virlet, P. Florian, and P. J. Grandinetti, *Solid State NMR* **6,** 73 (1996).
6. C. Fernandez and J-P. Amoureux, *Solid State NMR* **5,** 315 (1996).
7. S. Vega, T. W. Shattuck, and A. Pines, *Phys. Rev. Lett.* **37,** 43 (1976).
8. S. Vega and A. Pines, *J. Chem. Phys.* **66,** 5624 (1977).
9. S. Vega, *J. Chem. Phys.* **68,** 5518 (1978).
10. S. Vega and Y. Naor, *J. Chem. Phys.* **75,** 75 (1981).
11. A. Wokaun and R. R. Ernst, *J. Chem. Phys.* **67,** 1752 (1977).
12. A. Samoson, E. Lippmaa, and A. Pines, *Mol. Phys.* **65,** 1013 (1988).
13. A. Llor and J. Virlet, *Chem. Phys. Lett.* **152,** 248 (1988).
14. A. Bax, N. M. Szeverenyi, and G. E. Maciel, *J. Magn. Reson.* **52,** 147 (1983).
15. T. Terao, H. Miura, and A. Saika, *J. Chem. Phys.* **85,** 3816 (1986).
16. B. F. Chmelka, K. T. Mueller, A. Pines, J. Stebbins, Y. Wu, and J. W. Zwanziger, *Nature* **339,** 42 (1989).
17. K. T. Mueller, B. Q. Sun, G. C. Chingas, J. W. Zwanziger, T. Terao, and A. Pines, *J. Magn. Reson.* **86,** 470 (1990).
18. G. Bodenhausen, H. Kogler, and R. R. Ernst, *J. Magn. Reson.* **58,** 370 (1984).
19. C. Schmidt, B. Blumich, and H. W. Spiess, *J. Magn. Reson.* **79,** 269 (1988).
20. R. R. Ernst, G. Bodenhausen, and A. Wokaun, ''Principles of Nuclear Magnetic Resonance in One and Two Dimensions,'' Clarendon Press, Oxford, 1990.
21. M. H. Levitt, D. P. Raleigh, F. Creuzet, and R. G. Griffin, *J. Chem. Phys.* **92,** 6347 (1990).
22. M. J. Duer and M. H. Levitt, *Solid State NMR* **1,** 211 (1992).
23. N. C. Nielsen, H. Bildsoe, and H. J. Jakobsen, *Chem. Phys. Lett.* **191,** 205 (1992).
24. A. Samoson, E. Kundla, and E. Lippmaa, *J. Magn. Reson.* **49,** 350 (1982).
25. A. Samoson and E. Lippmaa, *J. Magn. Reson.* **84,** 410 (1989).
26. J-P. Amoureux, *Solid State NMR* **2,** 83 (1993).
27. M. M. Maricq and J. S. Waugh, *J. Chem. Phys.* **70,** 330 (1979).
28. V. H. Schmidt, ''Pulsed Magnetic and Optical Resonance. Proceedings of the 1971 Ampere International Summer School II'' (R. Blinc, Ed.), University of Ljubljiana, Yugoslavia, 1972.
29. M. Bloom, J. H. Davis, and M. I. Valic, *Can. J. Phys.* **58,** 1510 (1980).
30. A. Samoson and E. Lippmaa, *Phys. Rev. B* **28,** 6567 (1983).

31. A. Samoson and E. Lippmaa, *Chem. Phys. Lett.* **100,** 205 (1983).

32. D. Fenzke, D. Freude, T. Frohlich, and J. Haase, *Chem. Phys. Lett.* **111,** 171 (1984).

33. L. Pandey, S. Towta, and D. G. Hughes, *J. Chem. Phys.* **85,** 6923 (1986).

34. P. P. Man, J. Klinowski, A. Trokiner, H. Zanni, and P. Papon, *Chem. Phys. Lett.* **151,** 143 (1988).

35. G. J. Bowden and W. D. Hutchison, *J. Magn. Reson.* **67,** 403 (1986).

36. G. J. Bowden, W. D. Hutchison, and J. Khachan, *J. Magn. Reson.* **67,** 415 (1986).

37. A. Weiss, *Z. Naturforsch. A* **15,** 536 (1960).